ISSN:2229-6107

INTERNATIONAL JOURNAL OF PURE AND APPLIED SCIENCE & TECHNOLOGY

E-mail :
editor.ijpast@gmail.com
editor@ijpast.in

www.ijpast.in

INTERNATIONAL JOURNAL OF PURE AND APPLIED SCIENCE & TECHNOLOGY
IJPAST

ISSN 2229-6107 www.ijpast.in

Vol 13,Issuse 2.May 2023

A ROBUST CONTINUOUD TIME MPC OF A DC-DC BOOST CONVERTER INTERFACED WITH A GRID CONNECTED PV SYSTEM AND PR CONTROLLER

[1]V. BRAMHAM YADAV,[2]B. HARSHITHA,[3]B. SREEYA,[4]G. VARSHITHA

Abstract

The main function of the dc-dc converter in a gridconnected photovoltaic system, is to regulate the terminal voltage of the PV arrays to ensure delivering the maximum power to the grid. The purpose of this paper is to design and practically implement a robust continuous-time model predictive control (CTMPC) for a dc-dc boost converter, feeding a three-phase inverter of a grid-connected PV system to regulate the PV output voltage. In CTMPC, the system behavior is predicted based on Taylor series expansion, raising concerns about the prediction accuracy in the presence of parametric uncertainty and unknown external disturbances. To overcome this drawback, a disturbance observer is designed and combined with CTMPC to enhance the steady-state performance in the presence of model uncertainty and unknown disturbance such as the PV current, which varies nonlinearly with the operating point. An interesting feature is that the composite controller reduces to a conventional PI controller plus a predictive term that allow to further improve the dynamic performance over the whole operating range. The effectiveness of the proposed controller was tested numerically and validated experimentally with the consideration of the gridconnected PV inverter system and its controller

INTRODUCTION

In order to make the most of PV power production in either grid-connected or stand-alone applications, power electronic converters are required. Focusing on grid-connected applications, the PV unit is often linked to the host grid through a DC-link capacitor and a single/three phase inverter. In addition, a dc-dc converter and PV array are often connected with an input capacitor [1]. The inverter's primary function is to ensure that the PV system's power flow is controlled and within grid standards. Active power is managed by adjusting the DC-link voltage in such a topology [2], while reactive power is kept within a range that is determined primarily by the need to connect to the grid [3]. By investigating the switching devices' control potential, the dc-dc converter is thought to allow for the highest possible power to be extracted from the PV generator [4]. Boost converters have largely supplanted other dc-dc converters as the go-to for powering grid-connected inverters. Unlike other dc-dc converters, such as a quadrature boost converter or an interleaved boost converter [5, 6], the main benefit of utilizing a boost converter is its comparatively simple architecture. Boost converters are often used in low-power single-phase systems, however the DC-link voltage fluctuations they create are a matter for worry. Despite the fact that this issue highlights the need of creating an adequate control of the grid-tied single-phase inverter system, the primary emphasis of this work is on the control of the boost converter regardless of the inverter type. However, for some low power PV applications like the residential PV installed system, a three-phase inverter may provide smaller DC-link ripples with a conventional Proportional-Integral (PI) controller.

[1]ASSISTANT PROFESSOR, [2,3&4]UG SCHOLAR
DEPARTMENT OF EEE,
MALLA REDDY ENGINEERING COLLEGE FOR WOMEN, HYDERABAD

This is why the suggested controller for a dc-dc boost converter is being evaluated on the performance of a three-phase grid-tied inverter in this study. However, all the findings in this research may be extrapolated to single-phase PV systems that are linked to the grid.A traditional cascaded approach is frequently used for dc-dc boost converter control because to its simplicity, which facilitates controller design and practical implementation. A slower outer-loop provides a reference value, or the current reference, to a faster inner-loop as part of the cascaded control method. The latter is intended to regulate the PV array's terminal voltage, and its target value is often set using an MPPT algorithm [7].

MODELLING OF SYSTEMS

As shown in Figure 1, a dc-dc boost converter, three-phase inverter, and line filter (consisting of an inductance L and a resistance R), all connect to the ac bus. Switching devices S1, S6, and S7 are controlled to maintain a constant DC-link voltage vdc. The goal of this project is to use the switching actions of the semiconductor device Sb to control the PV output voltage v0. Input capacitor Cb and boost inductor Lb are indicated here. The inductor current iL and the PV voltage v0 are the primary parameters that may be monitored in a boost converter. The control law takes into account the voltage vdc as a known disturbance, whereas the current ip is treated as an unknown disturbance that must be calculated and accounted for.

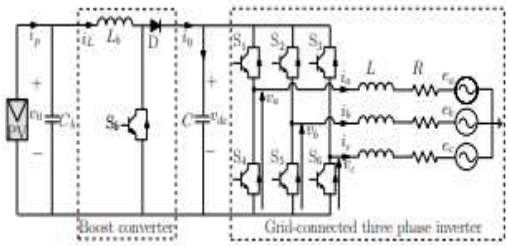

Fig. 1. Schematic diagram of a PV three-phase conversion system.

Assuming that the converter operates in a continuous conduction mode, then, the dynamics of the boost converter depicted in Fig. 1 can be described by the following set of differential equations

$$\begin{cases} \dfrac{di_L}{dt} = \dfrac{v_0}{L_b} - \dfrac{v_{dc}}{L_b} + \dfrac{v_{dc}}{L_b}d \\ \dfrac{dv_0}{dt} = -\dfrac{i_L}{C_b} + \dfrac{i_p}{C_b} \end{cases}$$

where d represent the duty-cycle control. In the cascaded scheme, the inner current control loop provides the dutycycle d, which is realized by means of a fixed frequency PWM. Making use of (1), the current controller can be designed based on the linear model of the current equation given by

$$\frac{di_L}{dt} = A_i i_L + B_i u_i + F_i b_i, \quad u_i = (d-1).$$

Where

$$A_i = 0,\ B_i = \frac{v_{dc}}{L_b},\ F_i = \frac{1}{L_b},\ b_i = v_0 + \delta_i$$

The term δi is added to the model to represent the lumped disturbances caused by model uncertainty. In the outer voltage loop, the current iL is treated as a control input. Thus, the current reference, for the inner-loop, can be determined from the outer-loop voltage control based on the following linear model

$$\frac{dv_0}{dt} = A_v v_0 + B_v u_v + F_v b_v, \quad u_v = i_L.$$

Where

$$A_v = 0,\ B_v = -\frac{1}{C_b},\ F_v = \frac{1}{C_b},\ b_v = i_p + \delta_v$$

The term δv represents parameter variations and external disturbances. In order to simplify the controller design, it is assumed that

$$\lim_{t\to\infty} \dot{\delta}_i(t) = 0, \qquad \lim_{t\to\infty} \dot{\delta}_v(t) = 0$$

ROBUST CONTINUOUS-TIME MODEL PREDICTIVE CONTROL (CTMPC)

Baseline Controller:

Formulation of CTMPC Consider a mathematical model for a single-input-singleoutput (SISO) disturbed linear system

$$\dot{y} = Ay + Bu + Fb$$

Where

$$u \in \mathbb{R},\ y \in \mathbb{R},\ \text{and}\ b \in \mathbb{R},$$

are the input, the output, and the disturbance, respectively. The continuous-time MPC is

essentially an optimal control that results from minimizing a quadratic cost function defined by

$$\Im = [e(t+T_r)]^2 = [y_r(t+T_r) - y(t+T_r)]^2$$

where, yr represents the output reference, e(t) is the tracking error, and Tr is known as predictive time. In the continuoustime MPC formulation, the control input is not usually included in the cost function to simplify the stability analysis. In such conditions, the control effort can be restricted by tuning the predictive time Tr or/and limiting the set-point changes. The optimal control is derived based on the optimality condition give

$$\frac{d\Im}{du} = 0$$

Following [18], the design methodology of a continuoustime MPC is based on approximating the future tracking error e(t + Tr) with the use of Taylor series expansion up to (ρ + r) th order, with r denotes the control order and ρ is the relative degree of the system. The main role of the control order is to ensure the stability of the closed-loop system for systems having high relative degree [25]. However, for the system under investigation, it is clear that the relative degree is equal to 1 for both loops. That is why, the control order r is set equal to be zero in this work. Hence, an approximate of e(t + Tr) is given by

$$e(t+T_r) = e(t) + T_r\dot{e}(t)$$

Making use of (7), from the definition of the relative degree ρ, it follows that

$$\dot{e}(t) = \dot{y}_r(t) - \dot{y} = \dot{y}_r(t) - Ay - Bu - Fb$$

Hence, (10) can be simplified as

$$e(t+T_r) = \Pi(T_r)(H(y) - Gu - Mb)$$

Where

$$\Pi = \begin{bmatrix} 1 & T_r \end{bmatrix}, \quad H(y) = \begin{bmatrix} e(t) & \dot{y}_r(t) - Ay \end{bmatrix}^T$$

The column matrices G and M are given by

$$G = \begin{bmatrix} 0 \\ B \end{bmatrix}, \quad M = \begin{bmatrix} 0 \\ F \end{bmatrix}$$

Invoking (13)–(14), and replacing e(t + Tr) in (8) by its expression given by (12), the approximate cost function = can be expressed as foll

$$\Im = (H(y) - Gu - Mb)^T \Upsilon(T_r)(H(y) - Gu - Mb)$$

ASSIMILATIONS ON COMPUTERS

diagram of a control loop

The control block schematic for the dc-dc boost converter and the three-phase grid-connected inverter are both shown in Figure 2. The literature reports a cascaded structure of PI controllers as the standard control method for a three-phase grid-connected inverter. The DC-link voltage is regulated by the outer-loop, which utilizes the d-axis current id as a control input, while the d- and q-axis currents are regulated by the inner-loop, which employs the voltage components vd and vq. The voltage instructions v d and v q are then transformed into the three-phase voltage commands v a, v b, and v c that may be implemented using PWM methods. In order to keep the power factor at 1, the q-axis current, iq, should be kept constant at 0. To acquire the components in the synchronous rotating frame (d, q), a phase-locked loop (PLL) technique is used to create the reference angle in order to keep eq = 0 [28], where eq represents the voltage along the q-axis of the grid. The grid voltage ed along the d-axis will so coincide with the grid voltage vector. According to [29], the inner-loop PI controller's Kpi and Kii coefficients may be designed as Kpi = 2LniR and Kii = L2 ni, while the outer-loop PI controller's Kpv and Kiv coefficients can be found as Kpv = 2Cnv and Kiv = C2 nv, where represents the damping factor.

natural angular frequency (ni,v) is represented by the ratio. Taking the switching frequency into account, a common value for is 1 2, while ni,v may be chosen to provide a settling time of, say, 4 ni,v. One thing to keep in mind while designing a cascaded scheme is that the outer-loop should be made to react more slowly than the inner-loop. A single diode PV panel model created in [31] is used in MATLAB/SIMULINK simulation experiments to illustrate the efficacy of the suggested technique. The maximum power point (MPP) of the PV panel under standard circumstances is 1 kW, and its I-V characteristic curve is shown in Fig. 3. The dc-dc boost converter's switching frequency (fsc) is set at 12.5 kilohertz, while the three-phase inverter's switching frequency (fsi) is 6.25 kilohertz. The 80 msec control period was used in the simulated experiments. The whole developed model has a time step of 1 picosecond.

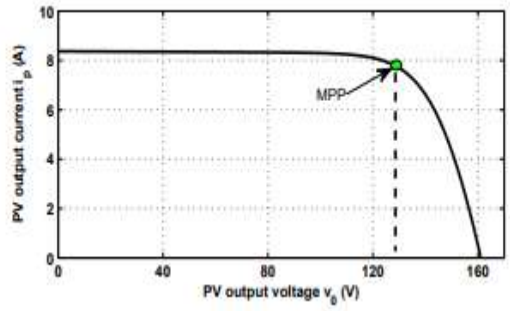

Fig. 2. Characteristic I–V curve of the PV array under standard conditions, with IMP P = 7.75 A, VMP P = 129 V, and PMP P = 1 kW.

Taking into account the minimum switching frequency fsc of the semiconductor device, the nominal specifications of the settling time tsc 4Tr, described by (21), may be used to derive the parameters of the proposed controller for the dc-dc boost converter. at provide a rapid and stable control under a cascaded structure, the predictive time Tr, the initial design consideration, is set at 0.2 ms for the inner-loop and 2 ms for the outer-loop. By adjusting the observer gains to i = 0.1, the settling time of the closed-loop current control is reduced to nine times the switching period Tsc = 1/fsc, which is sufficiently quick [27]. To keep the cascaded control scheme stable, the observer gain v should be maximized while keeping the response of the voltage control slower than that of the current control. This results in an outer-loop settling time that is five times as long as the inner-loop when the observer gain v is set to 0.5. In addition, a first-order linear filter with a time constant of Tr = 2 ms is utilized to realize the voltage reference and prevent overshoot due to the integral action in response to a step input. In this way, the nominal tracking performance is preserved while the transient inductor current is reduced and the steady-state error is eliminated. The Appendix contains the developed system's parameter values.

Monitoring Activity at Full Throttle The first experiment measured the system's ability to keep up with a sudden drop from 158 V to 130 V in the PV voltage reference. To get the most juice out of the PV panel, a voltage of 130 V was used. An experiment of this kind is analogous to a variation in the active power P supplied to the grid, with P = 0 1 kW.

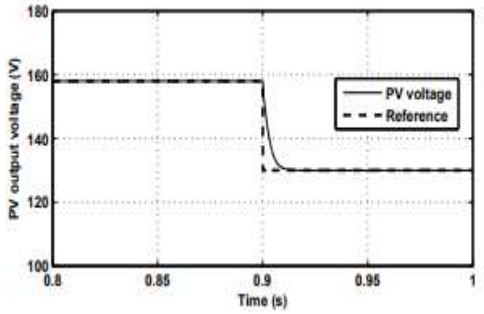

Fig. 3. PV output voltage response.

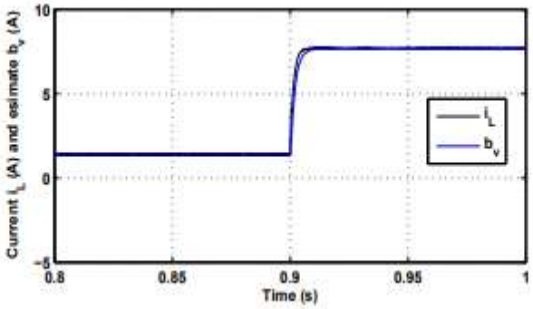

Fig 4 Inductor current and the disturbance estimation

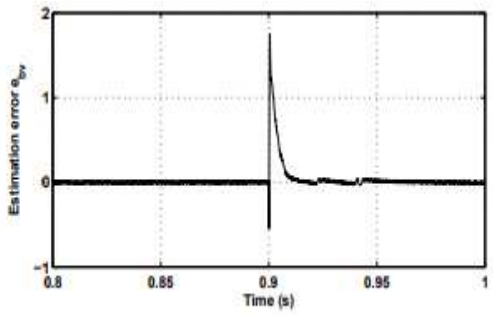

(b) Estimation error $e_{bv} = i_L - b_v$

Fig. 5. Inductor current response to a step change in v0.

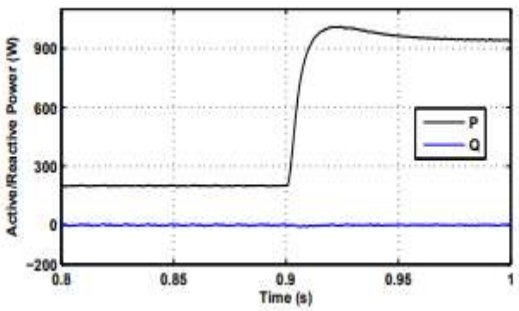

Fig. 6. Active and reactive powers delivered to the grid in response to a step change in v0

Even though the PV current ip fluctuates nonlinearly with the operating point, as seen in Figure 4, the PV output voltage followed its reference with 0% steady-state error. Since the current iL is equal to the unknown component ip in

the steady-state domain, Fig. 5 shows that the estimate bv followed the inductor current iL with an error that reduces to zero as time goes to infinity, suggesting that the disturbance observer is asymptotically stable. The inverter losses cause a steady-state inaccuracy in the active power P, as shown in Fig. 6, while the reactive power Q is held constant at zero.

Keeping Tabs on Progress Using a Moving Benchmark

The efficacy of the proposed controller over its entire working range was tested by subjecting it to a series of step adjustments in the PV output voltage. As v0ref = 158 145 135 120 V, the PV voltage was successfully reduced in stages from 158 V (near the open circuit value) to 120 V (below the MPP voltage). As well as this, progress was made upward.

as $v_{0ref} = 120 \rightarrow 135 \rightarrow 145 \rightarrow 158$ V.

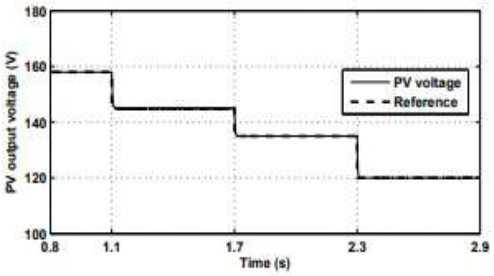

(a) PV output voltage response

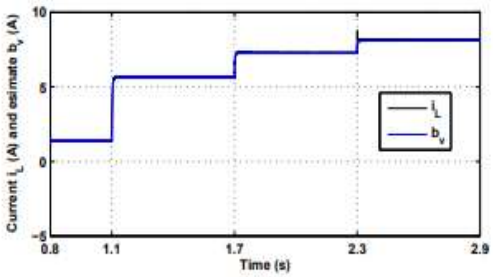

(b) Inductor current and the disturbance estimation b_v

Fig. 7. Tracking performance with downward steps of v0.

According to Figs. 7(a) and 8(a), the proposed controller allows achieving good transient and steady-state performances independently of the operating points. More interestingly, similar dynamic performance can be observed over the entire operating range. The inductor current iL, shown in Figs. 7(b) and 8(b), exhibits a good dynamic performance without a significant overshoot as the PV voltage changed due to the filtered PV voltage reference. Similarly to the previous test, the estimate bv closely followed the inductor current iL

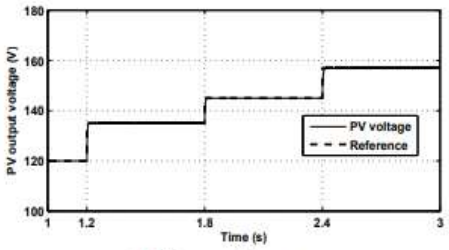

(a) PV output voltage response

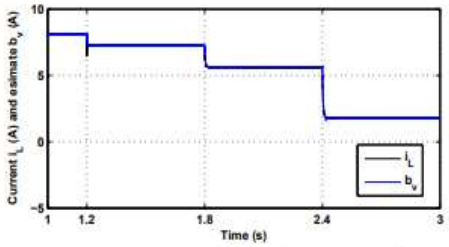

(b) Inductor current and the disturbance estimation b_v

Fig. 8. Tracking performance with upward steps of v0.

RESULTS OF EXPERIMENTS

Laboratory Environment

By connecting the dc-dc converter's output to a grid-connected inverter, as illustrated in Fig. 9, experimental testing were performed to evaluate the suggested controller while taking into account actual circumstances.

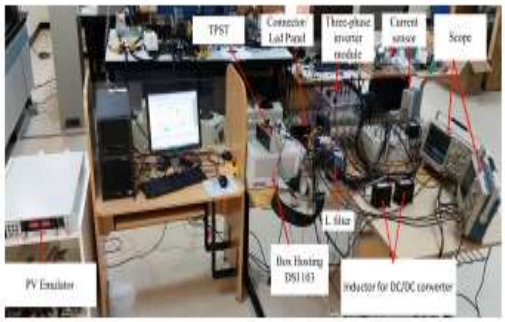

Fig. 9. Laboratory setup for testing the proposed controller

The input capacitor Cb, a dc-dc boost converter, a DC-link capacitor, a three-phase inverter, and a L type filter are all part of the experimental setup for simulating a PV system and injecting current into the grid with minimal ripple. Magna-Power Electronics' XR160-12 power supply module was utilized to generate the PV power with the I-V characteristic seen in Fig. 3. A six-pulse IGBT inverter and a dc-dc converter were built using a Semiteach power electronics module (AN 8005) from Semikron. The dSPACE ds1103 DSP board enabled the implementation of the predictive controller for the dc-dc converter and the proportional-integral (PI) controller for the grid-side inverter. The settings of the controller parameters, switching frequencies, and control

period are those used in the hardware realization. PV output voltage regulation with v = 0.5 is unstable, however, according to experimental results. At v = 0.5, the settling time of the voltage control approaches that of the current control, which unquestionably impacts the stability of the cascaded control system and may account for the discrepancy between the modeling and practical test. To deal with this, we set the observer gain v to 0.1, which results in an outer-loop settling time that is 12 times longer than the inner-loop's.

Monitoring Activity at Full Throttle

A step adjustment in PV voltage was applied to the dc-dc converter in this experiment to verify the initial simulation findings and guarantee the maximum possible power was sent to the grid. Figures 10 and 11 indicate the PV voltage regulation performance achieved from the experiments is very close to that obtained from the simulation test. The inductor's current response, however, is clearly slower than the result of the simulation test. An inherent responsiveness of the PV emulator to a quick change in PV voltage may account for the discrepancy between simulated and experimental findings.

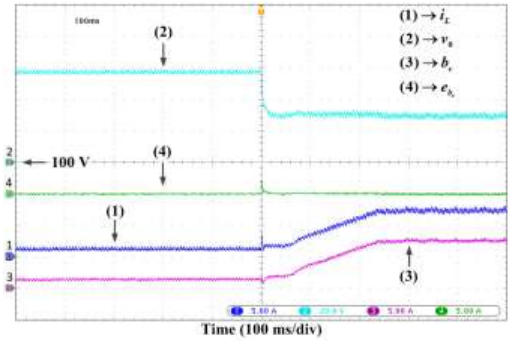

Fig. 10. Boost converter's response under a step input of PV voltage: v0(20 V/div), iL(5 A/div), bv(5 A/div), and ebv (5 A/div).

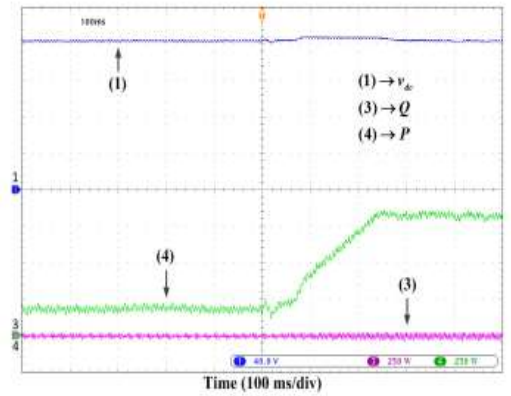

Fig. 11. DC-link voltage and active/reactive power delivered to the grid under a step input of PV voltage: vdc(40 V/div), P(250 W/div), and Q(250 W/div).

Also, it can be seen that the estimate bv tracked accurately the inductor current iL and the estimation error ebv converges to zero at the steady-state regime. For the grid-tied inverter control, it is clear that that the DC-link voltage and the reactive power Q are well controlled. Here, P represents the active transferred to the grid. The unity power factor operation is guaranteed as shown in Fig. 12. It is noted that the modulating signals m∗ a , m∗ b , and m∗ c are generated using third harmonic injection technique, so as to to prevent overmodulation problem.

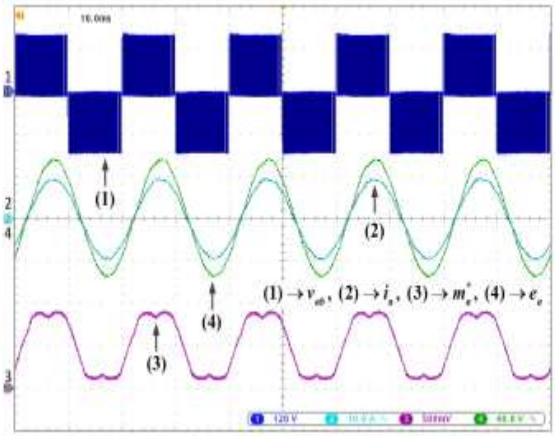

Fig. 12. Grid current ia, grid voltage ea, the voltage vab at the output of the inverter, and the reference of the modulating signal m∗a using the third harmonic injection technique: ia(10 A/div), ea(40 V/div), vab(120 V/div), and m∗a(0.5 V/div).

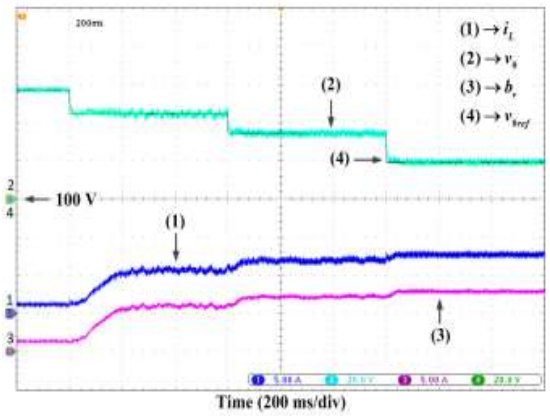

Fig. 13. Performance evaluation under downward steps of v0: v0(20 V/div), iL(5 A/div), and bv(5 A/div).

CONCLUSION

Many PV systems make use of a cascaded control scheme that includes a dc-dc boost converter feeding a grid-connected three-phase inverter. This work proposes a robust continuous-time model predictive control for this purpose. To reduce the steady-state error due to parametric uncertainty and unknown PV current, the disturbance observer enables for high tracking performance to be

achieved in response to a smooth reference. As a result, across the whole working range, the composite con troller provides superior transient and steady-state capabilities. The design process was also detailed in detail. For verifying the suggested controller's performance in light of real-world dynamics, a PI controller was also developed to regulate the grid-connected AC power converter. The modeling and experimental findings showed that the dc-dc boost converter was controlled effectively to enter a steady-state phase with high accuracy and strong dynamic performance over the whole working range.

REFERENCES

[1] J. Viinamäki, J. Jokipii, T. Messo, T. Suntio, M. Sitbon, and A. Kuperman, "Comprehensive dynamic analysis of photovoltaic generator interfacing dc–dc boost power stage," IET Renew. Power Gen., vol. 9, no. 4, pp. 306–314, 2015.

[2] M. Mahmud, H. Pota, and M. Hossain, "Dynamic stability of threephase grid-connected photovoltaic system using zero dynamic design approach," IEEE J. Photovolt., vol. 2, no. 4, pp. 564–571, Oct 2012.

[3] C. Y. Tang, Y. T. Chen, and Y. M. Chen, "PV power system with multimode operation and low-voltage ride-through capability," IEEE Trans. Ind Electron., vol. 62, no. 12, pp. 7524–7533, Dec 2015.

[4] P. Sharma and V. Agarwal, "Maximum power extraction from a partially shaded PV array using shunt-series compensation," IEEE J. Photovolt., vol. 4, no. 4, pp. 1128–1137, July 2014.

[5] Z. Chen, P. Yang, G. Zhou, J. Xu, and Z. Chen, "Variable duty cycle control for quadratic boost PFC converter," IEEE Trans. Ind Electron., vol. PP, no. 99, pp. 1–1, 2016.

[6] O. Lopez-Santos, L. Martinez-Salamero, G. Garcia, H. ValderramaBlavi, and T. Sierra-Polanco, "Robust sliding-mode control design for a voltage regulated quadratic boost converter," IEEE Trans. Power Electron., vol. 30, no. 4, pp. 2313–2327, April 2015.

[7] D. Sera, L. Mathe, T. Kerekes, S. V. Spataru, and R. Teodorescu, "On the perturb-and-observe and incremental conductance MPPT methods for PV systems," IEEE J. Photovolt., vol. 3, no. 3, pp. 1070–1078, July 2013.

[8] M. Villalva, T. de Siqueira, and E. Ruppert, "Voltage regulation of photovoltaic arrays: small-signal analysis and control design," IET Power Electron., vol. 3, no. 6, pp. 869–880, 2010.

[9] J. Thongpron, K. Kirtikara, and C. Jivacate, "A method for the determination of dynamic resistance of photovoltaic modules under illumination," Sol. Energy Mater. Sol. Cells, vol. 90, no. 18, pp. 3078–3084, 2006.

[10] L. Nousiainen, J. Puukko, A. Mäki, T. Messo, J. Huusari, J. Jokipii, J. Viinamäki, D. Lobera, S. Valkealahti, and T. Suntio, "Photovoltaic generator as an input source for power electronic converters," IEEE Trans. Power Electron., vol. 28, no. 6, pp. 3028–3038, 2013.

[11] A. Urtasun and D. Lu, "Control of a single-switch two-input buck converter for MPPT of two PV strings," IEEE Trans. Ind. Electron., vol. 62, no. 11, pp. 7051–7060, 2015.

[12] A. Urtasun, P. Sanchis, and L. Marroyo, "Adaptive voltage control of the dc/dc boost stage in PV converters with small input capacitor," IEEE Trans. Power Electron., vol. 28, no. 11, pp. 5038–5048, 2013.

[13] M. Sitbon, S. Schacham, and A. Kuperman, "Disturbance observer-based voltage regulation of current-mode-boost-converter-interfaced photovoltaic generator," IEEE Trans. Ind. Electron., vol. 62, no. 9, pp. 5776– 5785, 2015.

[14] M. Soroush and C. Kravaris, "A continuous-time formulation of nonlinear model predictive control," Int. J. Control, vol. 63, no. 1, pp. 121–146, 1996.

[15] P. J. Gawthrop, H. Demircioglu, and I. I. Siller-Alcala, "Multivariable continuous-time generalised predictive control: A state-space approach to linear and nonlinear systems," in IEE Proc. Control Theory Appl., vol. 145, no. 3. IET, 1998, pp. 241–250.

[16] W.-H. Chen, D. J. Ballance, P. J. Gawthrop, J. J. Gribble, and J. O'Reilly, "Nonlinear PID predictive controller," IEE Proc. Control Theory Appl., vol. 146, no. 6, pp. 603–611, 1999.

[17] J. Yang and W. X. Zheng, "Offset-free nonlinear MPC for mismatched disturbance attenuation with application to a static var compensator," IEEE Trans. Circuits Sys. II: Express Briefs, vol. 61, no. 1, pp. 49–53, Jan 2014.

[18] J. Yang, W. Zheng, S. Li, B. Wu, and M. Cheng, "Design of a prediction accuracy enhanced continuous-time MPC for disturbed systems via a disturbance observer," IEEE Trans. Ind. Electron., vol. 62, no. 9, pp. 5807–5816, 2015.

[19] R. Errouissi, M. Ouhrouche, W.-H. Chen, and A. M. Trzynadlowski, "Robust cascaded nonlinear predictive control of a permanent magnet synchronous motor with antiwindup compensator," IEEE Trans. Ind. Electron., vol. 59, no. 8, pp. 3078–3088, 2012.